

Review

# High Entropy Alloys Manufactured by Additive Manufacturing

José M. Torralba <sup>1,2,\*</sup>  and Mónica Campos <sup>1</sup> 

<sup>1</sup> Department of Materials Science and Engineering, School of Engineering, Universidad Carlos III de Madrid, 28911 Leganés, Spain; campos@ing.uc3m.es

<sup>2</sup> IMDEA Materials Institute, 28906 Getafe, Spain

\* Correspondence: josemanuel.torralba@uc3m.es; Tel.: +34-91-626-9916

Received: 13 April 2020; Accepted: 12 May 2020; Published: 15 May 2020



**Abstract:** High entropy alloys have attracted much interest over the last 16 years due to their promising unusual properties in different fields that offer many new possible applications. Additionally, additive manufacturing has drawn attention due to its versatility and flexibility ahead of a new material challenge, being a suitable technology for the development of metallic materials. Moreover, high entropy alloys have demonstrated that many gaps exist in the literature on its physical metallurgy, and in this sense, additive manufacturing could be a feasible technology for solving many of these challenges. In this review paper the newest literature on this topic is condensed into three different aspects: the different additive manufacturing technologies employed to process high entropy alloys, the influence of the processing conditions and composition on the expected structure and microstructure and information about the mechanical and corrosion behavior of these alloys.

**Keywords:** high entropy alloys; additive manufacturing; microstructural development; corrosion; refractory HEAs

## 1. High Entropy Alloys

High entropy alloys (HEAs) are a new family of metallic materials that have attracted important attention in the last 16 years since they first appeared in the scientific literature in 2004 with two key papers that introduced the concept of these alloys [1,2]. Since the publication of those papers, this materials engineering field has increased enormously, and today, more than 10,000 papers and patents related to this topic have been published; additionally, different subbranches such as “refractory high entropy alloys” [3] and “eutectic high entropy alloys” have emerged [4]. In recent years, many interesting and well detailed review papers [5,6] have been written on this topic, including books [7]. A highly comprehensive review was also recently published [8].

HEAs were first developed via ingot metallurgy, but in this family of alloys, which uses five or more elements and many with dissimilar density, it is difficult to obtain a good level of solubility during melting and to avoid segregation during solidification. In this case, powder metallurgy (PM) is a forming technology that can avoid many problems present in conventional ingot metallurgy, offering a better microstructural control, the possibility of nanocrystalline materials or the capability of developing metal matrix composites without the segregation issue. The first papers related to HEAs manufactured by PM appeared in 2008 [9–11]. Since the early days of this new family of structural alloys, the benefits of nanostructures and their potential uses in many applications have been highlighted [1]. PM is similar to other forming techniques such as high-pressure torsion, but has some particular advantages [12], including two particular benefits over other forming techniques: (1) it can be applied when metals with dissimilar densities must be used, which is the case when lightweight HEAs are developed [13] and (2) it can be applied when many metals with notably high melting points

are involved, the so-called refractory HEAs [3]. Recently, a comprehensive review has been published on PM and HEAs [14] with a deep analysis of the PM manufacturing routes, the alloying elements used in development and the properties of the PM materials compared with ingot casting HEAs. In this decade, more than 300 papers have been published on high entropy alloys manufactured by PM techniques; more than 50 of these papers report an additive manufacturing approach (not including the use of powders to develop laser cladding coatings).

## 2. Additive Manufacturing and High Entropy Alloys

Additive Manufacturing (AM) is a group of technologies that build 3D objects by adding layer-upon-layer of material. With this technology can be obtained parts made in polymer, composites, ceramics, metals and even human tissue [15]. In the context of AM of metals, we can classify the main processing methods in three groups: powder bed systems, powder feed systems and binder-based systems. AM of metals can also be obtained by wire feed systems. We can find in the literature excellent reviews focused on AM of metals, where the technologies are extensively described and also the microstructural development and properties related to the most extended structural alloys (stainless steels, high strength steels, high speed steels, titanium, aluminum, nickel, etc.) [16–18]. In [19] is developed a processing guide where we can find criterium to select one specific technology and in [17] are also business considerations and comparison with alternative powder metallurgy methods. Most powder bed and powder feed methods are based in laser technologies, and in [20], can be found a good review to the technological problems related to these technologies. In 2017 and 2018 where published two comprehensive reviews on HEAs manufactured by AM [21,22]. Up to this time, near 30 papers were published on the topic. Since those papers were published, in 2019 and 2020 were published another 40 papers, so the present study try to be an update of the information published on the topic and avoiding overlapping with the previous reviews published.

If we consider the published works on HEAs and additive manufacturing (AM) (Figure 1), most of the works can be divided into three main technologies, two based on the powder bed system (selective laser melting and electron beam melting) and one based on powder feed system (laser direct deposition). Most of papers published based on the later system used the “laser engineered net shaping” (LENS) technology. This use means that approximately half of the published works used a powder bed technique and the other half used a powder feed technique. Only two papers were found on HEAs manufactured on binder-based additive manufacturing techniques [23,24]. In Table 1 is summarized this distribution of technologies. The above mentioned review study on this topic [22] emphasizes on the physical metallurgy of the AM HEAs.

**Table 1.** AM systems and technologies (data from [10–12,15,16]) used for HEAs (number of papers).

AM Systems	Powder Bed	Powder Feed	Binder-Based
Technologies	EBM (5) SLM (23)	DMD (19) LENS (10)	Binder-jetting (1) Polyjet (1)

Raw materials used in AM of metals is a key issue. The selection of the powder with the required specific characteristics for each technology is a key factor for the good development of the part. Today, taking into account the price of the powder devoted to AM, the recycling of the powders during the manufacturing cycle is also an important matter [25]. In the powder bed systems, is mandatory to use fully prealloyed powders (usually gas atomized) and in powder feed and binder-based systems can be used both fully prealloyed and elemental mix of powders.

If we analyze the published papers, approximately half of them address the Cantor alloy (CA) [2], which is an equi-atomic alloy composed of CoCrFeMnNi. This coverage could be a consequence of the scarce availability of pre-alloyed gas atomized powders in the market, which forces use of the most-studied alloy, especially in the case of the powder bed systems in which fully alloyed powders are a must. Approximately 30% of the papers report modifications of the Cantor alloy with different

additions of Al. As it will be discussed later, Al is a strong BCC stabilizer; this can allow a lot of possible dual microstructures (FCC-BCC) opening to the heat treatments the possibility of improving the mechanical properties.

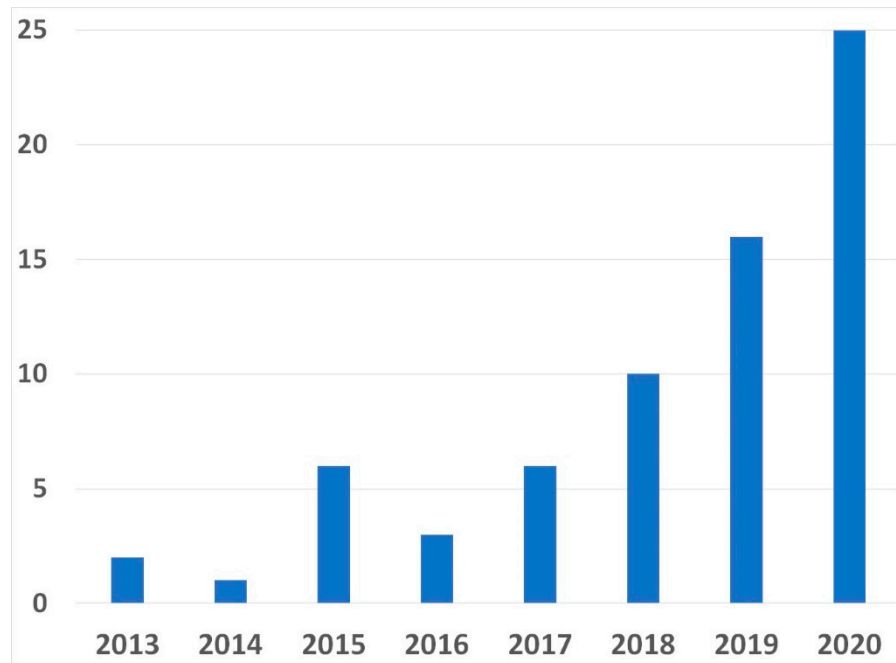


**Figure 1.** Papers published on high entropy alloys (HEAs) by additive manufacturing (AM) (year 2020 papers published up to April 2020).

Figure 2 shows an analysis of the frequency of the alloying elements used in the different technologies and the most used the core group of elements of the CA (Fe, Ni, Cr and Co). Figure 3 illustrates the percentage of studies using the different alloying approaches employed in additive manufacturing.

The as-cast CA shows a dendritic FCC microstructure [26]. The addition of Al can promote a dendritic structure in which the FCC dendrites are surrounded by an interdendritic BCC phase. Depending on the heat treatment, the microstructural morphology can change and this change influences the properties [27], as discussed later. The morphologic changes are always linked with the treatment temperature and the cooling rate and can modify the dendritic microstructure into granular and for high cooling rates into a refinement of the dendritic structure. Beyond the CA and the CA modified by Al, others investigations have shown the effect of replacing alloying elements in CA composition by other transition elements, such as Cu or Ti. Finally, five papers address the refractory HEAs, all obtained by direct metal deposition (Figures 2 and 3).

The following sections analyze selected obtained properties and the use of further heat treatments or final treatments such as hot isostatic pressing.

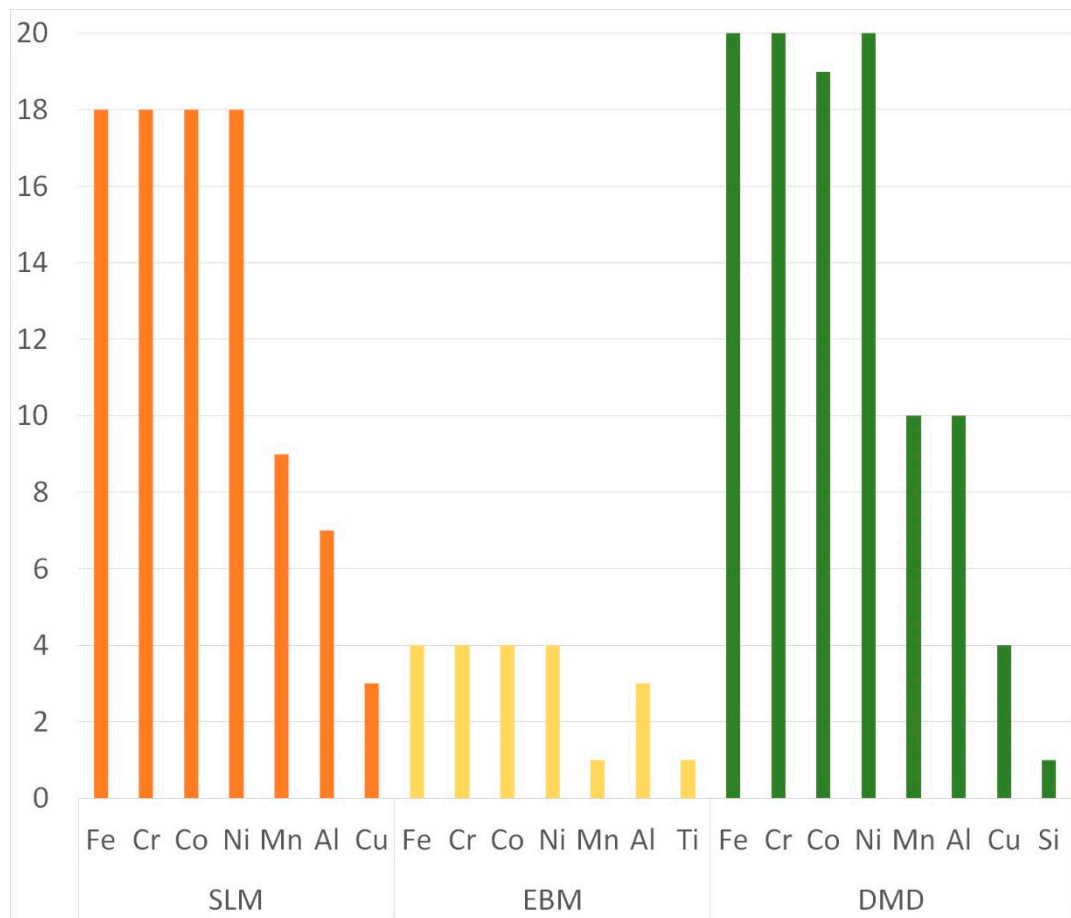


Figure 2. Frequency (number of papers) of elements used in the AM HEAs.

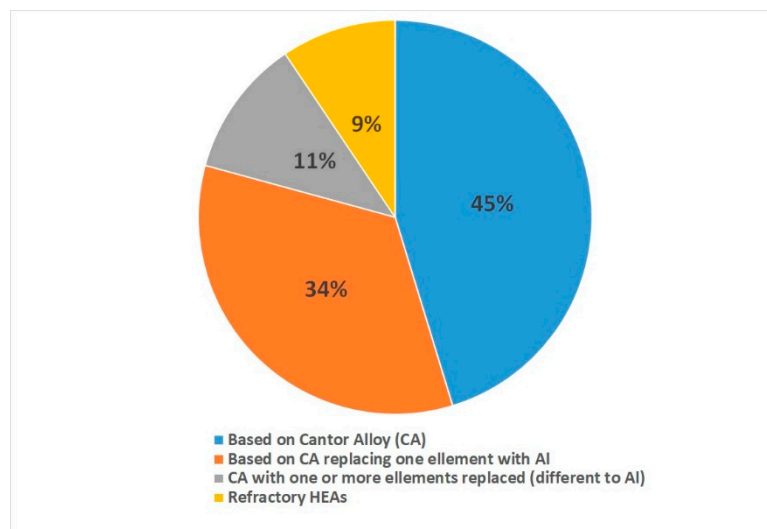


Figure 3. Types of alloys present in AM processes.

### 3. Microstructural Analysis of the Additive Manufactured Alloys

If we analyze the microstructural study conducted in those papers in which the CA was used, it is clear that the microstructures develop through an FCC single phase and follow, in some sense, what could be predicted in a conventional ingot solidification process. In fact, during any of the two main AM processes (powder bed or powder feed), the powder is fully melted and solidified on a substrate that acts as a large heat sink. This solidification process takes place in a small space, and its evolution

depends on the conditions of the process: the energy of the laser beam, cooling speed, temperature of the substrate, etc. In some cases [28–32], the authors only report a columnar microstructure with grains growing along the built direction. Other authors refer to the presence of a cellular structure (far from the equiaxed structure) that can be transformed into an equiaxed structure through an annealing process [33,34]. In most cases, the columnar structure coexists with equiaxed grains [35–39], especially in the final step of the solidification pool or near the walls of the solidification area, where columnar and equiaxed grains can progress together. Figure 4 summarizes the microstructural appearance of the “as built” state when a laser method is used. In Figure 4a, we observe a typical epitaxial configuration in which the columnar structure is developed in the built direction and is transformed into random columnar (b), granular (c) or nearly equiaxed (d) grains depending on the position and the cooling rate.

If we modify the selected processing conditions, this situation can change slightly. Heat treatments or cooling rates [33,40] can promote a greater amount of equiaxed grains, and higher beam energy promotes higher equiaxed grains [41].

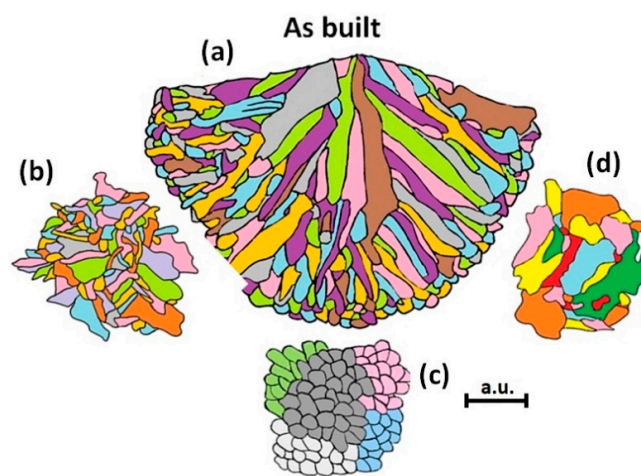


**Figure 4.** Microstructural approach through a schematic illustration (made from [37,39,42–45]) of the Cantor alloy manufactured by laser additive manufacturing methods in the “as built” condition. (a) Epitaxial configuration with columnar grains in the built direction, (b) random columnar grains, (c) granular grains and (d) nearly equiaxed grains. The magnification mark is arbitrary due to the different papers used but is in the range of 40–80  $\mu\text{m}$ .

These are a subset of the possibilities, because the number of variables in the process (including the building speed or the energy of the beam) can modify the microstructure in many aspects. These microstructural features also can be changed via an annealing treatment. If we anneal the “as built” alloy, as shown in Figure 5, the microstructure tends to evolve into different situations: grain growth, evolution to equiaxed grains and development of twins.

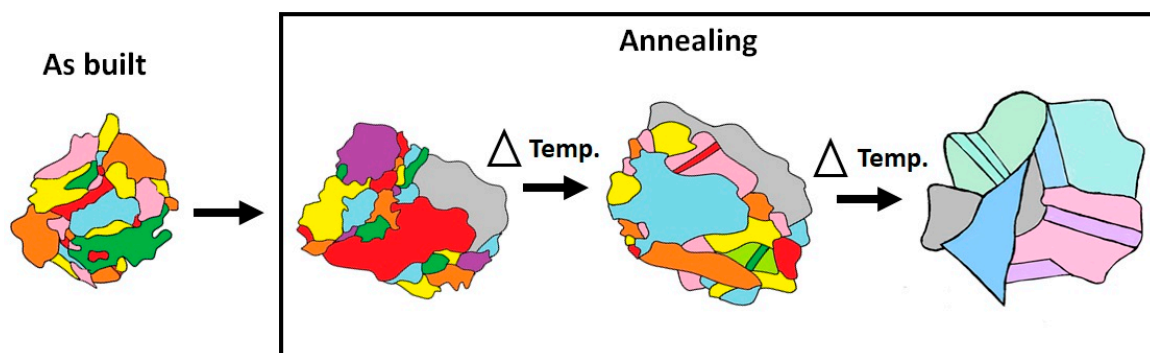


**Figure 5.** Microstructural evolution of the Cantor alloy from the “as built” state after annealing.

More than 1/3 of considered papers, focus on modified CA by the replacement of Mn by Al to a certain extent. Since the Al is a clear BCC stabilizer, depending on the amount of Al, and occasionally with a proportional decrease in the Ni content, the microstructural development is based on the development of a BCC (disordered) structure in conjunction with an ordered BCC phase (B2). When the amount of Al is less than 10% (at.), i.e., in the stoichiometric composition of  $Al_{0.3}CoCrFeNi$ , the obtained structure fully remains FCC [46–48]. Once the amount of Al reaches the stoichiometric composition of  $Al_{0.5}CoCrFeNi$ , B2/BCC phases can be found [43,49,50], and with more than this amount of Al, even  $\sigma$  phase can be detected [51]. The sequence of the phases appears from the liquid state and according to the thermodynamic studies as follows. The first phase in the solidification process is the ordered B2 ( $L \rightarrow L + B2$ ) followed by the disordered BCC ( $L + B2 \rightarrow L + B2 + BCC \rightarrow B2 + BCC$ ).

Solidification takes place with B2 + BCC phases (near 1560 °C). At lower temperatures (about 1520 °C), the FCC precipitates surrounding as a matrix like a net [52,53]. When temperature reaches values near 1200 °C (the preheating temperature in the EBM process)  $\sigma$  phase can be also precipitated. In [53], the authors studied the relationship among the three phases in the “as built” alloy, where the presence of the FCC phase is greatly reduced. That work also compared an EBM process wherein any condition that could be considered far from the equilibrium situation, allows a lower amount of the FCC phase. The presence of a B2/BCC phase in combination with FCC could be an advantage in the design of the final properties because it can allow to develop heat treatments where the final microstructure can be customized in some extent to obtain some specific properties.

Figure 6 compares the different aspects in the microstructure of the “as built”  $AlCoCrFeNi$  alloy with the same material obtained in EBM at two different cooling conditions. In all cases, the B2 phase is formed (since B2 has the highest melting temperature is the first to solidified, this phase is the first to form), followed by the precipitation of a dendritic BCC phase and finally, an FCC phase is established in the grain boundaries of the B2 phase. The work in [43] fully analyzed the elemental segregation via atom probe tomography, showing how Ni and Al are segregated in the interdendritic B2, meanwhile Fe and Cr do in the dendritic BCC phase (for SLM processing method).

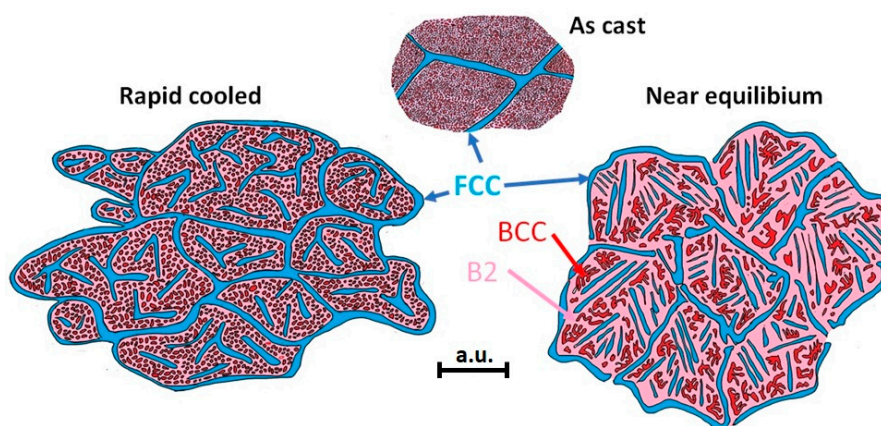


**Figure 6.** Microstructural approach through a schematic illustration (made from [24,51,53–59]) for the “as built”  $AlCoCrFeNi$  and EBMed near the equilibrium conditions and rapid cooled. The magnification mark is arbitrary due to the different papers used, but is in the range of 2–15  $\mu m$ .

The amount of B2/BCC relative to the FCC phase can be regulated through the relationship in the composition between Al and Ni [48,51] and through proper heat treatments after AM manufacturing. The higher the annealing temperature is, the greater the amount of FCC phase that can be found in the microstructure [24,57]. To avoid the presence of  $\sigma$  phase, which can have a negative effect for some properties (such as corrosion behavior), the alloy can be quenched from the annealing temperature [57]. Hot isostatic pressing can also be used to improve the properties of 3D printed specimens [59] and to stabilize the FCC phase also (when a single phase is pursued). This later work proposes a continuous

cooling–transformation diagram to avoid formation of the  $\sigma$  phase and to predict the amount of the B2-BCC/FCC relationship for the  $\text{Al}_{0.85}\text{CoCrFeNi}$  alloy.

In certain papers, CA composition is redefined through the partial replacement of Mn by Al and Cu. In those papers, when the amount of Ni exceeds the average in the alloy, the predominant microstructure is based on FCC plus ordered BCC (B2) [55,56] (SLM and LENS, respectively). FCC is always located in the grain boundaries, and B2 appears in a form similar to an interdendritic phase, where Cu plays an important role because it used to be segregated in the B2 phase. When the amounts of Al and Ni are in a good balance, BCC is the formed microstructure, with the prevalence of the B2 ordered phase [60] (LENS). The FCC phase is precipitated at the grain boundaries only after annealing at high temperature (FCC phases were precipitated in larger quantities in the sample that was heat-treated at 1000 °C) [54] (SLM).

It was mentioned the possible presence of  $\sigma$  phase in this family of  $\text{Al}_x\text{CoCrFeNi}$  HEAs. The proposed microstructural analysis can be modified slightly by this presence, but in order to offer a comprehensive model, it was simplified not including it in the proposed prototypes. Despite the analysis of the  $\sigma$  phase is not studied in deep in AM HEAs, it has been widely analyzed in ingot metallurgy (or other powder metallurgy process) HEAs with similar composition [61,62].

Special mention could be made in the analysis presented in [38]. In this study, a base alloy of  $\text{Al}_x\text{CuCrFeNi}_2$  (where the  $x$  value ranges from 0.8 to 1) (Figure 7) is used to analyze the microstructural evolution with attention to the predominant phase during solidification (through LENS process). In this study, a deep thermodynamic study of the  $\text{AlCuCrFeNi}$  system is performed by analyzing the ternary diagrams grouping the elements by Ni-Cu-Cr, Ni-Cu-Fe and Ni-Fe-Cr. It is interesting to note the calculated isopleth for  $\text{Al}_x\text{CrCuFeNi}_2$  (with  $x = 0$  to 2) showing possible phases as a function of Al content and particularly the primary field change with increasing amount of Al added to the  $\text{CrCuFeNi}_2$  alloy, as shown in Figure. For lower amounts of Al, primary solidification promotes the formation of FCC and at lower temperatures, a B2 phase can be precipitated, usually by spinodal decomposition ( $\text{BCC} \rightarrow \text{BCC} + \text{B2}$ ), where Cu is highly concentrated in the B2 interdendritic phase. However, for higher amounts of Al is the other way around, primary solidification takes place to produce a B2 structure and at lower temperatures, a FCC phase is precipitated in the grain boundaries. This study also explains why the increase in Al content changes the primary solidification phase from a FCC to a FCC + BCC to a BCC-based microstructure. This microstructural transition is attributed to the relatively large size of the Al atoms compared with those of Co, Fe, Cr and Ni atoms, as also confirmed in [63,64]. Consequently, the large size misfit within the FCC lattice forces it to adopt a BCC structure [65,66].

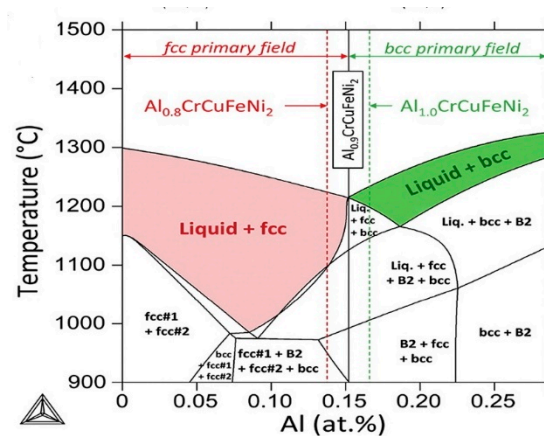


**Figure 7.** Isopleth for  $\text{Al}_x\text{CrCuFeNi}_2$  (with  $x = 0$ –2) showing possible phases as a function of Al content and particularly the primary field change with increasing amount of Al added to the  $\text{CrCuFeNi}_2$  alloy. Data from [58].

A number of papers have been published on the use of refractory high entropy alloys (see chapter 6). In this case, a BCC structure is always developed [42,67–69]

An interesting microstructural analysis of the MA HEAs is also made in the above mentioned study [22]. From this analysis the authors classify this family of alloys in four specific groups: CoCrFeNi,  $\text{Al}_x\text{CoCrFeNi}$ , CoCrFeMnNi and  $\text{Ti}_{25}\text{Zr}_{50}\text{Nb}_0\text{Ta}_5$ .

#### 4. Tensile Features of Additive Manufactured HEAs

In most published papers on HEAs manufactured by conventional powder route, there is a lack of information regarding to the tensile features of the specimens created by these technologies. But considering this review of additive manufacturing, many studies exist with relevant results on tensile features. Most of these investigations have obtained the data from parts processed by SLM [38,44,45,49,56,70–75], although there are some others that explored the tensile behavior over EBM materials [40,52,75,76] or processed by DMD methods [28–30,33,35,37].

Figure 8 displays the tensile features from all of these researches, without considering the state of the material (as built or after heat treatment) with the aim of constructing a frame to understand what we can expect from these technologies. Most of the additive manufactured HEAs attained a tensile strength (TS) in the range of 600–800 MPa, but with strain values that can reach 50%.

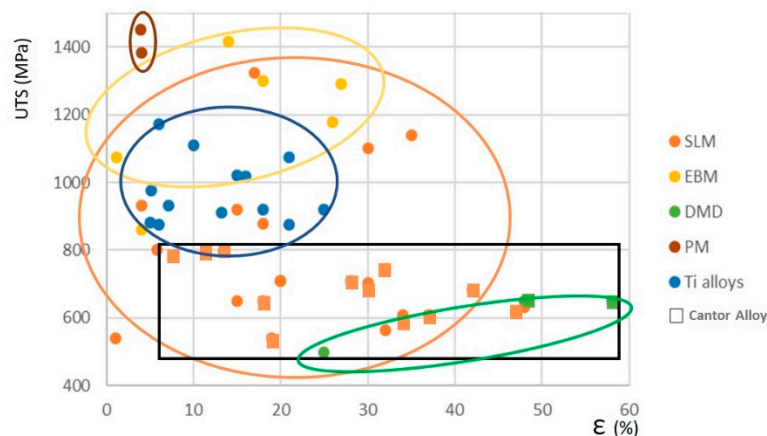


**Figure 8.** Tensile features of selected HEAs obtained by different additive manufacturing routes, after [28–30,33,35,38,40,44,45,49,52,56,70–79]. In the black square and also highlighted with square dots are confined most of the plain CAs.

EBM materials (and a subset by SLM) can exceed TS over 1100 MPa but with lower strain. Just the opposite of those specimens obtained by DMD which achieve lower TS values but higher strain levels (up to 60%, but with a small sample of tests). The figure shows how most of the Cantor alloys belong to the selective laser melting process. What we can conclude from this figure is the versatility of these technologies in obtaining materials with many different balances between strength and elongation. Figure also displays selected results related to HEAs obtained by other alternative powder metallurgy routes [77,78] and a fair few high-strength AM titanium base alloys [79,80] to have the reference of some other structural competing alloys with the HEAs and also two references of other hot pressed HEAs [77,78].

The Cantor alloy manufactured by SLM also exhibits good tensile features (900 MPa, 35% elongation) at cryogenic temperatures (77 K) [28].

In [22] is made a deep study on the mechanical properties of the AM HEAs. One of the conclusions of this review is the fact that there is a lack of knowledge in the mechanical properties of this materials, being an opportunity to develop new researches to provide new sets of mechanical properties, to allow new AM HEAs suitable for a complex service environment.

## 5. Corrosion Behavior of Additive Manufactured HEAs

A few studies have determined the corrosion behavior of HEAs manufactured by additive manufacturing. The high level of Cr in these alloys could presuppose a good corrosion behavior. The first approach was attempted with the Cantor alloy [33] or the Cantor alloy modified with Al [52–57]. In the Cantor alloy, where the microstructure is FCC, the presence of Mn reduces the chance of good corrosion behavior and produces pitting corrosion in the adjacent areas with coexistence of Mn-rich areas with Ni-rich areas. In the case of AlCoFeNiCr alloys, where Mn is replaced by Al, the analysis was conducted on materials after annealing at high temperature, which promoted a microstructure in which FCC coexists with BCC-B2 phases in all of the cases. The polarization diagrams of these alloys exhibit slightly worse behavior of HEAs compared with that of conventional wrought stainless steels. This type of microstructure, in which an FCC phase coexists and is usually enriched in Fe and Cr with BCC-B2 phases enriched in Al and Ni produces severe pitting corrosion that degrades the behavior of these materials, with the B2 phases acting as an anodic agent against FCC, which acts as a cathode. The microstructural constraints that harm the corrosion behavior of HEAs are different than those that affect to the AM stainless steels, that usually are related to the formation of  $(Cr,Mo)_7C_3$  carbides [80]. Comparison between HEAs and stainless steels in terms of corrosion, seems to be the most appropriate, but the amount of information regarding HEAs and corrosion is much lower. Stainless steels is one of the first materials to be used at industrial level in AM, so there are a lot of information about these family of steels [81]. But some valuable information from the corrosion behavior of AM stainless steels can be exported to AM HEAs: the strong relationship of the AM process conditions and the corrosion behavior. This is due to the significant influence of the processing parameters, the density and grain size [82] and the improvement of these properties with the heat treatments [83].

Far beyond the conventional HEAs, we find a study with the alloy CoCrFeNiTi (where Ti replaces the Mn) in which the pitting–corrosion potential (for materials obtained by both EBM and SLM) are much better than those of the conventional high corrosion-resistant alloys, such as duplex stainless steels and Ni-based superalloys used in harsh corrosive environments [75]. This good behavior is even demonstrated despite the possible formation of  $Ni_3Ti$  intermetallic compounds, which are Cr-depleted zones that can preferentially cause pitting corrosion. Some special HEAs such as AlCoFeNiTiV<sub>0.9</sub>Sm<sub>0.1</sub> and AlCoFeNiV<sub>0.9</sub>Sm<sub>0.1</sub> have shown a corrosion behavior that can be competitive with stainless steels [84].

## 6. Refractory High Entropy Alloys

Creation of refractory HEAs presents selected difficulties, but essentially, two main challenges exist: 1) refractory metals have a high affinity for oxygen; any treatment should be sufficiently shielded to avoid oxidation and 2) the notably high melting temperatures of these elements. From these two important restrictions, it is easy to understand that additive manufacturing as an emerging technology for high entropy alloys reveals that not many scientific works were produced. In fact, a few studies were found and three of them are preliminary feasibility studies without any pretension of fulfilling a required property. In all cases, the DMD technique was used as the building method; thanks to DMD technology the HEA is obtained from elemental powders. From these group of works it can be highlighted the following three. In [85] a HEA is built from elemental powders, where it was mixed elements with three levels of melting points (Mo, Nb and Ta over 2400 °C, Cr at 1907 °C and Al, at 660); despite some evaporation problems with the Al, the selective EBM processing method is suitable to develop such a complex alloy from elemental powders. In [86] is obtained a complete map of microstructures, obtained by building by DMD several compositions maintaining three fix elements (MoNbTa, MoNbW and NbTaW) and varying from null the fourth one (W, Nb and No, respectively). Laser powder feed methods allows to construct these kinds of materials where we can analyze from the same process run, many possibilities in different properties using the same set of alloying elements. And in [87] using four elements (Mo, Nb, Ta and W) and combining modeling with

the linear combination of the four elements is demonstrated the suitability of the DMD method to develop different complex alloys.

Other publications [67,88] studied the viability of obtaining two refractory HEAs (TiZrNbMoV, ZrTiVCrFeNi), but in this case, a specific property and application is desired. In both cases, a successful process was followed and the obtained alloys showed a good capability to absorb and de-absorb hydrogen in a cyclic manner with small losses in the full cycle. The authors in [68,69] studied the feasibility of building three refractory HEAs (MoNbTaW, TiZrNbTa, TiZrNbHfTa) by DMD. In all cases, a good homogeneous mixing of the elements was obtained, despite the high melting points (and high differences in the melting points), and in all cases, a homogeneous BCC structure was found. This knowledge offers new possibilities for AM in this field of materials.

## 7. Summary and Possible Future Developments

Both high entropy alloys and additive manufacturing have recently attracted substantial interest. High entropy alloys have revealed a new field in metallurgical engineering due to the emerging possibilities with respect to the expected properties. Additionally, new paradigms in terms of phenomena must be explained under this new philosophy of alloying methods. However, metal additive manufacturing offers numerous challenges for metallurgical engineering because many problems that arise during the development of a new material must be solved. In combining the two topics, we face a new and exciting field to be explored. As explained in this review, until now, only a few different alloys have been available in the literature to discuss, but the versatility of the additive manufacturing technologies, especially those related to direct laser deposition, show that the starting point is not necessary for a pre-alloyed powder. These AM technologies open a wide field of research because many different alloys can be developed starting from elemental powders. AM can also be tailored to different microstructural configurations, opening to heat treatments, as a consequence to different tailored properties that could fulfill requirements for many different applications. This topic presents a large and open field that must be investigated to demonstrate the suitability of additive manufacturing as a forming technology for this family of materials.

After reviewing the topic, there is room for many research matters:

- (1) Alloying development. As has been highlighted, only a few traditional HEAs (near the Cantor alloy) were processed by AM. There are many possibilities to develop HEAs for customized applications by alloying design, especially with the versatility of the powder feed systems, where mix of elemental powders can be used. In this sense an interesting field is the so call eutectic HEAs and more combinations of refractory HEAs.
- (2) Heat treatments developments. The complex peculiarity of the AM technology combined with the complex physical metallurgy of the HEAs makes the heat treatments an open and promising field to develop better materials using this technology. In the analyzed papers only a few modalities of heat treatments were used. The possibility of having in the microstructure, at least, two different phases (BCC ordered and disordered and FCC) open an interesting field to research through the heat treatments.
- (3) Modeling. Today there are many computational tools to develop alloys in one specific processing method using multiscale modeling. AM has a lot of technological drawbacks that can be overcome thanks to this possibility. This recommendation also applies to the alloy development using thermodynamic modeling.
- (4) Characterization. Like in all new fields (and the combination of HEAs and AM) is an emerging field, there are many lacks of information regarding the knowledge in many fields of properties (dynamic mechanical properties, high temperature behavior, corrosion performance, magnetic properties, among others). This is another interesting field to new researches.

**Author Contributions:** J.M.T. and M.C. have participated equally in writing-review and editing the manuscript. All authors have read and agreed to the published version of the manuscript.

**Funding:** This research received no external funding.

**Conflicts of Interest:** The authors declare no conflict of interest.

## Abbreviations

HEAs	High entropy alloys
PM	Powder metallurgy
AM	Additive manufacturing
SLM	Selective laser melting
EBM	Electron beam melting
DMD	Direct metal deposition
LENS	Laser engineering net-shaping
CA	Cantor alloy
FCC	Face-centered cubic
BCC	Body-centered cubic

## References

1. Yeh, J.-W.; Chen, S.-K.; Lin, S.-J.; Gan, J.-Y.; Chin, T.-S.; Shun, T.-T.; Tsau, C.-H.; Chang, S.-Y. Nanostructured High-Entropy Alloys with Multiple Principal Elements: Novel Alloy Design Concepts and Outcomes. *Adv. Eng. Mater.* **2004**, *6*, 299–303. [[CrossRef](#)]
2. Cantor, B.; Chang, I.T.H.; Knight, P.; Vincent, A.J.B. Microstructural development in equiatomic multicomponent alloys. *Mater. Sci. Eng. A* **2004**, *375–377*, 213–218. [[CrossRef](#)]
3. Senkov, O.N.; Wilks, G.B.; Miracle, D.B.; Chuang, C.P.; Liaw, P.K. Refractory high-entropy alloys. *Intermetallics* **2010**, *18*, 1758–1765. [[CrossRef](#)]
4. Lu, Y.; Dong, Y.; Guo, S.; Jiang, L.; Kang, H.; Wang, T.; Wen, B.; Wang, Z.; Jie, J.; Cao, Z.; et al. A Promising New Class of High-Temperature Alloys: Eutectic High-Entropy Alloys. *Sci. Rep.* **2014**, *4*, 6200. [[CrossRef](#)] [[PubMed](#)]
5. Miracle, D.B.; Senkov, O.N. A critical review of high entropy alloys and related concepts. *Acta Mater.* **2017**, *122*, 448–511. [[CrossRef](#)]
6. Yeh, J.-W. Alloy Design Strategies and Future Trends in High-Entropy Alloys. *JOM* **2013**, *65*, 1759–1771. [[CrossRef](#)]
7. Murty, B.S.; Yeh, J.-W.; Ranganathan, S. *High Entropy Alloys*; Elsevier: Amsterdam, The Netherlands, 2019; ISBN 978-0-12-816067-1.
8. George, E.P.; Raabe, D.; Ritchie, R.O. High-entropy alloys. *Nat. Rev. Mater.* **2019**, *4*, 515–534. [[CrossRef](#)]
9. Varalakshmi, S.; Kamaraj, M.; Murty, B.S. Synthesis and characterization of nanocrystalline AlFeTiCrZnCu high entropy solid solution by mechanical alloying. *J. Alloys Compd.* **2008**, *460*, 253–257. [[CrossRef](#)]
10. Zhang, K.B.; Fu, Z.Y.; Zhang, J.Y.; Shi, J.; Wang, W.M.; Wang, H.; Wang, Y.C.; Zhang, Q.J. Nanocrystalline CoCrFeNiCuAl high-entropy solid solution synthesized by mechanical alloying. *J. Alloys Compd.* **2009**, *485*, L31–L34. [[CrossRef](#)]
11. Chen, Y.-L.; Hu, Y.-H.; Tsai, C.-W.; Hsieh, C.-A.; Kao, S.-W.; Yeh, J.-W.; Chin, T.-S.; Chen, S.-K. Alloying behavior of binary to octonary alloys based on Cu–Ni–Al–Co–Cr–Fe–Ti–Mo during mechanical alloying. *J. Alloys Compd.* **2009**, *477*, 696–705. [[CrossRef](#)]
12. Koch, C.C. Nanocrystalline high-entropy alloys. *J. Mater. Res.* **2017**, *32*, 3435–3444. [[CrossRef](#)]
13. Kumar, A.; Gupta, M. An Insight into Evolution of Light Weight High Entropy Alloys: A Review. *Metals* **2016**, *6*, 199. [[CrossRef](#)]
14. Torralba, J.M.; Alvaredo, P.; García-Junceda, A. High-entropy alloys fabricated via powder metallurgy. A critical review. *Powder Metall.* **2019**, *62*, 84–114. [[CrossRef](#)]
15. Singh, S.; Ramakrishna, S.; Singh, R. Material issues in additive manufacturing: A review. *J. Manuf. Process.* **2017**, *25*, 185–200. [[CrossRef](#)]
16. Herzog, D.; Seyda, V.; Wycisk, E.; Emmelmann, C. Additive manufacturing of metals. *Acta Mater.* **2016**, *117*, 371–392. [[CrossRef](#)]

17. Frazier, W.E. Metal Additive Manufacturing: A Review. *J. Mater. Eng. Perform.* **2014**, *23*, 1917–1928. [[CrossRef](#)]
18. Wong, K.V.; Hernandez, A. A Review of Additive Manufacturing. *ISRN Mech. Eng.* **2012**, *2012*, 208760. [[CrossRef](#)]
19. Gokuldoss, P.K.; Kolla, S.; Eckert, J. Additive Manufacturing Processes: Selective Laser Melting, Electron Beam Melting and Binder Jetting—Selection Guidelines. *Materials* **2017**, *10*, 672. [[CrossRef](#)]
20. Lee, H.; Lim, C.H.J.; Low, M.J.; Tham, N.; Murukeshan, V.M.; Kim, Y.-J. Lasers in additive manufacturing: A review. *Int. J. Precis. Eng. Manuf. Technol.* **2017**, *4*, 307–322. [[CrossRef](#)]
21. Cui, W.; Zhang, X.; Liou, F. Additive Manufacturing of High-Entropy Alloys—A Review. In Proceedings of the 28th Annual International Solid Freeform Fabrication Symposium—An Additive Manufacturing Conference, Austin, TX, USA, 7–9 August 2017; pp. 712–724.
22. Chen, S.; Tong, Y.; Liaw, P.K. Additive manufacturing of high-entropy alloys: A review. *Entropy* **2018**, *20*, 937. [[CrossRef](#)]
23. Kenel, C.; Casati, N.P.M.; Dunand, D.C. 3D ink-extrusion additive manufacturing of CoCrFeNi high-entropy alloy micro-lattices. *Nat. Commun.* **2019**, *10*, 904. [[CrossRef](#)] [[PubMed](#)]
24. Karlsson, D.; Lindwall, G.; Lundbäck, A.; Amnebrink, M.; Boström, M.; Riekehr, L.; Schuisky, M.; Sahlberg, M.; Jansson, U. Binder jetting of the AlCoCrFeNi alloy. *Addit. Manuf.* **2019**, *27*, 72–79. [[CrossRef](#)]
25. Cordova, L.; Campos, M.; Tinga, T. Revealing the Effects of Powder Reuse for Selective Laser Melting by Powder Characterization. *JOM* **2019**, *71*, 1062–1072. [[CrossRef](#)]
26. Cantor, B. Multicomponent and High Entropy Alloys. *Entropy* **2014**, *16*, 4749–4768. [[CrossRef](#)]
27. Shivam, V.; Basu, J.; Pandey, V.K.; Shadangi, Y.; Mukhopadhyay, N.K. Alloying behaviour, thermal stability and phase evolution in quinary AlCoCrFeNi high entropy alloy. *Adv. Powder Technol.* **2018**, *29*, 2221–2230. [[CrossRef](#)]
28. Qiu, Z.; Yao, C.; Feng, K.; Li, Z.; Chu, P.K. Cryogenic deformation mechanism of CrMnFeCoNi high-entropy alloy fabricated by laser additive manufacturing process. *Int. J. Light. Mater. Manuf.* **2018**, *1*, 33–39. [[CrossRef](#)]
29. Guan, S.; Wan, D.; Solberg, K.; Berto, F.; Welo, T.; Yue, T.M.; Chan, K.C. Additive manufacturing of fine-grained and dislocation-populated CrMnFeCoNi high entropy alloy by laser engineered net shaping. *Mater. Sci. Eng. A* **2019**, *761*, 138056. [[CrossRef](#)]
30. Xiang, S.; Li, J.; Luan, H.; Amar, A.; Lu, S.; Li, K.; Zhang, L.; Liu, X.; Le, G.; Wang, X.; et al. Effects of process parameters on microstructures and tensile properties of laser melting deposited CrMnFeCoNi high entropy alloys. *Mater. Sci. Eng. A* **2019**, *743*, 412–417. [[CrossRef](#)]
31. Amar, A.; Li, J.; Xiang, S.; Liu, X.; Zhou, Y.; Le, G.; Wang, X.; Qu, F.; Ma, S.; Dong, W.; et al. Additive manufacturing of high-strength CrMnFeCoNi-based High Entropy Alloys with TiC addition. *Intermetallics* **2019**, *109*, 162–166. [[CrossRef](#)]
32. Haase, C.; Tang, F.; Wilms, M.B.; Weisheit, A.; Hallstedt, B. Combining thermodynamic modeling and 3D printing of elemental powder blends for high-throughput investigation of high-entropy alloys – Towards rapid alloy screening and design. *Mater. Sci. Eng. A* **2017**, *688*, 180–189. [[CrossRef](#)]
33. Melia, M.A.; Carroll, J.D.; Whetten, S.R.; Esmaeely, S.N.; Locke, J.; White, E.; Anderson, I.; Chandross, M.; Michael, J.R.; Argibay, N.; et al. Mechanical and Corrosion Properties of Additively Manufactured CoCrFeMnNi High Entropy Alloy. *Addit. Manuf.* **2019**, *29*, 100833. [[CrossRef](#)]
34. Xu, Z.; Zhang, H.; Li, W.; Mao, A.; Wang, L.; Song, G.; He, Y. Microstructure and nanoindentation creep behavior of CoCrFeMnNi high-entropy alloy fabricated by selective laser melting. *Addit. Manuf.* **2019**, *28*, 766–771. [[CrossRef](#)]
35. Chew, Y.; Bi, G.J.; Zhu, Z.G.; Ng, F.L.; Weng, F.; Liu, S.B.; Nai, S.M.L.; Lee, B.Y. Microstructure and enhanced strength of laser aided additive manufactured CoCrFeNiMn high entropy alloy. *Mater. Sci. Eng. A* **2019**, *744*, 137–144. [[CrossRef](#)]
36. Luo, R.; Yang, Y.; Bian, H.; Chen, L.; Ouyang, L.; Peng, C.-T.; Gao, P.; Xu, G.; Cheng, X. High Temperature Deformation Characteristics of an Alumina-Forming Stainless Steel. *steel Res. Int.* **2019**, *90*, 1900022. [[CrossRef](#)]
37. Tong, Z.; Ren, X.; Jiao, J.; Zhou, W.; Ren, Y.; Ye, Y.; Larson, E.A.; Gu, J. Laser additive manufacturing of FeCrCoMnNi high-entropy alloy: Effect of heat treatment on microstructure, residual stress and mechanical property. *J. Alloys Compd.* **2019**, *785*, 1144–1159. [[CrossRef](#)]
38. Brif, Y.; Thomas, M.; Todd, I. The use of high-entropy alloys in additive manufacturing. *Scr. Mater.* **2015**, *99*, 93–96. [[CrossRef](#)]

39. Piglione, A.; Dovggy, B.; Liu, C.; Gourlay, C.M.; Hooper, P.A.; Pham, M.S. Printability and microstructure of the CoCrFeMnNi high-entropy alloy fabricated by laser powder bed fusion. *Mater. Lett.* **2018**, *224*, 22–25. [[CrossRef](#)]
40. Wang, P.; Huang, P.; Ng, F.L.; Sin, W.J.; Lu, S.; Nai, M.L.S.; Dong, Z.L.; Wei, J. Additively manufactured CoCrFeNiMn high-entropy alloy via pre-alloyed powder. *Mater. Des.* **2019**, *168*, 107576. [[CrossRef](#)]
41. Xiang, S.; Luan, H.; Wu, J.; Yao, K.-F.; Li, J.; Liu, X.; Tian, Y.; Mao, W.; Bai, H.; Le, G.; et al. Microstructures and mechanical properties of CrMnFeCoNi high entropy alloys fabricated using laser metal deposition technique. *J. Alloys Compd.* **2019**, *773*, 387–392. [[CrossRef](#)]
42. Kuncce, I.; Polanski, M.; Karczewski, K.; Plocinski, T.; Kurzydowski, K.J. Microstructural characterisation of high-entropy alloy AlCoCrFeNi fabricated by laser engineered net shaping. *J. Alloys Compd.* **2015**, *648*, 751–758. [[CrossRef](#)]
43. Karlsson, D.; Marshal, A.; Johansson, F.; Schuisky, M.; Sahlberg, M.; Schneider, J.M.; Jansson, U. Elemental segregation in an AlCoCrFeNi high-entropy alloy – A comparison between selective laser melting and induction melting. *J. Alloys Compd.* **2019**, *784*, 195–203. [[CrossRef](#)]
44. Zhu, Z.G.; Nguyen, Q.B.; Ng, F.L.; An, X.H.; Liao, X.Z.; Liaw, P.K.; Nai, S.M.L.; Wei, J. Hierarchical microstructure and strengthening mechanisms of a CoCrFeNiMn high entropy alloy additively manufactured by selective laser melting. *Scr. Mater.* **2018**, *154*, 20–24. [[CrossRef](#)]
45. Lin, D.; Xu, L.; Jing, H.; Han, Y.; Zhao, L.; Minami, F. Effects of annealing on the structure and mechanical properties of FeCoCrNi high-entropy alloy fabricated via selective laser melting. *Addit. Manuf.* **2020**, *32*, 101058. [[CrossRef](#)]
46. He, J.Y.; Liu, W.H.; Wang, H.; Wu, Y.; Liu, X.J.; Nieh, T.G.; Lu, Z.P. Effects of Al addition on structural evolution and tensile properties of the FeCoNiCrMn high-entropy alloy system. *Acta Mater.* **2014**, *62*, 105–113. [[CrossRef](#)]
47. Joseph, J.; Stanford, N.; Hodgson, P.; Fabijanic, D.M. Tension/compression asymmetry in additive manufactured face centered cubic high entropy alloy. *Scr. Mater.* **2017**, *129*, 30–34. [[CrossRef](#)]
48. Joseph, J.; Jarvis, T.; Wu, X.; Stanford, N.; Hodgson, P.; Fabijanic, D.M. Comparative study of the microstructures and mechanical properties of direct laser fabricated and arc-melted Al<sub>x</sub>CoCrFeNi high entropy alloys. *Mater. Sci. Eng. A* **2015**, *633*, 184–193. [[CrossRef](#)]
49. Sun, K.; Peng, W.; Yang, L.; Fang, L. Effect of SLM Processing Parameters on Microstructures and Mechanical Properties of Al<sub>0.5</sub>CoCrFeNi High Entropy Alloys. *Metals* **2020**, *10*, 292. [[CrossRef](#)]
50. Luo, S.; Gao, P.; Yu, H.; Yang, J.; Wang, Z.; Zeng, X. Selective laser melting of an equiatomic AlCrCuFeNi high-entropy alloy: Processability, non-equilibrium microstructure and mechanical behavior. *J. Alloys Compd.* **2019**, *771*, 387–397. [[CrossRef](#)]
51. Sistla, H.R.; Newkirk, J.W.; Frank Liou, F. Effect of Al/Ni ratio, heat treatment on phase transformations and microstructure of Al<sub>x</sub>FeCoCrNi<sub>2-x</sub> (x = 0.3, 1) high entropy alloys. *Mater. Des.* **2015**, *81*, 113–121. [[CrossRef](#)]
52. Kuwabara, K.; Shiratori, H.; Fujieda, T.; Yamanaka, K.; Koizumi, Y.; Chiba, A. Mechanical and corrosion properties of AlCoCrFeNi high-entropy alloy fabricated with selective electron beam melting. *Addit. Manuf.* **2018**, *23*, 264–271. [[CrossRef](#)]
53. Shiratori, H.; Fujieda, T.; Yamanaka, K.; Koizumi, Y.; Kuwabara, K.; Kato, T.; Chiba, A. Relationship between the microstructure and mechanical properties of an equiatomic AlCoCrFeNi high-entropy alloy fabricated by selective electron beam melting. *Mater. Sci. Eng. A* **2016**, *656*, 39–46. [[CrossRef](#)]
54. Zhang, M.; Zhou, X.; Wang, D.; Zhu, W.; Li, J.; Zhao, Y.F. AlCoCuFeNi high-entropy alloy with tailored microstructure and outstanding compressive properties fabricated via selective laser melting with heat treatment. *Mater. Sci. Eng. A* **2019**, *743*, 773–784. [[CrossRef](#)]
55. Borkar, T.; Gwalani, B.; Choudhuri, D.; Mikler, C.V.; Yannetta, C.J.; Chen, X.; Ramanujan, R.V.; Styles, M.J.; Gibson, M.A.; Banerjee, R. A combinatorial assessment of Al<sub>x</sub>CrCuFeNi<sub>2</sub> (0 <x <1.5) complex concentrated alloys: Microstructure, microhardness, and magnetic properties. *Acta Mater.* **2016**, *116*, 63–76.
56. Luo, S.; Zhao, C.; Su, Y.; Liu, Q.; Wang, Z. Selective laser melting of dual phase AlCrCuFeNi<sub>x</sub> high entropy alloys: Formability, heterogeneous microstructures and deformation mechanisms. *Addit. Manuf.* **2020**, *31*, 100925. [[CrossRef](#)]
57. Wang, R.; Zhang, K.; Davies, C.; Wu, X. Evolution of microstructure, mechanical and corrosion properties of AlCoCrFeNi high-entropy alloy prepared by direct laser fabrication. *J. Alloys Compd.* **2017**, *694*, 971–981. [[CrossRef](#)]

58. Choudhuri, D.; Gwalani, B.; Gorsse, S.; Mikler, C.V.; Ramanujan, R.V.; Gibson, M.A.; Banerjee, R. Change in the primary solidification phase from fcc to bcc-based B2 in high entropy or complex concentrated alloys. *Scr. Mater.* **2017**, *127*, 186–190. [[CrossRef](#)]
59. Joseph, J.; Hodgson, P.; Jarvis, T.; Wu, X.; Stanford, N.; Fabijanic, D.M. Effect of hot isostatic pressing on the microstructure and mechanical properties of additive manufactured AlxCoCrFeNi high entropy alloys. *Mater. Sci. Eng. A* **2018**, *733*, 59–70. [[CrossRef](#)]
60. Welk, B.A.; Williams, R.E.A.; Viswanathan, G.B.; Gibson, M.A.; Liaw, P.K.; Fraser, H.L. Nature of the interfaces between the constituent phases in the high entropy alloy CoCrCuFeNiAl. *Ultramicroscopy* **2013**, *134*, 193–199. [[CrossRef](#)]
61. Cieslak, J.; Tobola, J.; Berent, K.; Marciszko, M. Phase composition of AlxFeNiCrCo high entropy alloys prepared by sintering and arc-melting methods. *J. Alloys Compd.* **2018**, *740*, 264–272. [[CrossRef](#)]
62. Sliwa, P.; Berent, K.; Przewoznik, J.; Cieslak, J. Mössbauer investigations of the  $\sigma$ -phase in the AlxCrFeCoNi high entropy alloys. *J. Alloys Compd.* **2020**, *814*, 151757. [[CrossRef](#)]
63. Zhang, Y.; Zuo, T.T.; Tang, Z.; Gao, M.C.; Dahmen, K.A.; Liaw, P.K.; Lu, Z.P. Microstructures and properties of high-entropy alloys. *Prog. Mater. Sci.* **2014**, *61*, 1–93. [[CrossRef](#)]
64. Tong, C.-J.; Chen, Y.-L.; Yeh, J.-W.; Lin, S.-J.; Chen, S.-K.; Shun, T.-T.; Tsau, C.-H.; Chang, S.-Y. Microstructure characterization of AlxCoCrCuFeNi high-entropy alloy system with multiprincipal elements. *Metall. Mater. Trans. A* **2005**, *36*, 881–893. [[CrossRef](#)]
65. Zhang, C.; Zhang, F.; Chen, S.; Cao, W. Computational Thermodynamics Aided High-Entropy Alloy Design. *JOM* **2012**, *64*, 839–845. [[CrossRef](#)]
66. Guo, S.; Ng, C.; Lu, J.; Liu, C.T. Effect of valence electron concentration on stability of fcc or bcc phase in high entropy alloys. *J. Appl. Phys.* **2011**, *109*, 103505. [[CrossRef](#)]
67. Kunce, I.; Polanski, M.; Bystrzycki, J. Microstructure and hydrogen storage properties of a TiZrNbMoV high entropy alloy synthesized using Laser Engineered Net Shaping (LENS). *Int. J. Hydrogen Energy* **2014**, *39*, 9904–9910. [[CrossRef](#)]
68. Dobbstein, H.; Gurevich, E.L.; George, E.P.; Ostendorf, A.; Laplanche, G. Laser metal deposition of a refractory TiZrNbHfTa high-entropy alloy. *Addit. Manuf.* **2018**, *24*, 386–390. [[CrossRef](#)]
69. Dobbstein, H.; Thiele, M.; Gurevich, E.L.; George, E.P.; Ostendorf, A. Direct Metal Deposition of Refractory High Entropy Alloy MoNbTaW. *Phys. Procedia* **2016**, *83*, 624–633. [[CrossRef](#)]
70. Agrawal, P.; Thapliyal, S.; Nene, S.S.; Mishra, R.S.; McWilliams, B.A.; Cho, K.C. Excellent strength-ductility synergy in metastable high entropy alloy by laser powder bed additive manufacturing. *Addit. Manuf.* **2020**, *32*, 101098. [[CrossRef](#)]
71. Wu, W.; Zhou, R.; Wei, B.; Ni, S.; Liu, Y.; Song, M. Nanosized precipitates and dislocation networks reinforced C-containing CoCrFeNi high-entropy alloy fabricated by selective laser melting. *Mater. Charact.* **2018**, *144*, 605–610. [[CrossRef](#)]
72. Li, R.; Niu, P.; Yuan, T.; Cao, P.; Chen, C.; Zhou, K. Selective laser melting of an equiatomic CoCrFeMnNi high-entropy alloy: Processability, non-equilibrium microstructure and mechanical property. *J. Alloys Compd.* **2018**, *746*, 125–134. [[CrossRef](#)]
73. Zhou, R.; Liu, Y.; Zhou, C.; Li, S.; Wu, W.; Song, M.; Liu, B.; Liang, X.; Liaw, P.K. Microstructures and mechanical properties of C-containing FeCoCrNi high-entropy alloy fabricated by selective laser melting. *Intermetallics* **2018**, *94*, 165–171. [[CrossRef](#)]
74. Fujieda, T.; Chen, M.; Shiratori, H.; Kuwabara, K.; Yamanaka, K.; Koizumi, Y.; Chiba, A.; Watanabe, S. Mechanical and corrosion properties of CoCrFeNiTi-based high-entropy alloy additive manufactured using selective laser melting. *Addit. Manuf.* **2019**, *25*, 412–420. [[CrossRef](#)]
75. Fujieda, T.; Shiratori, H.; Kuwabara, K.; Kato, T.; Yamanaka, K.; Koizumi, Y.; Chiba, A. First demonstration of promising selective electron beam melting method for utilizing high-entropy alloys as engineering materials. *Mater. Lett.* **2015**, *159*, 12–15. [[CrossRef](#)]
76. Sun, C.; Li, P.; Xi, S.; Zhou, Y.; Li, S.; Yang, X. A new type of high entropy alloy composite Fe<sub>18</sub>Ni<sub>23</sub>Co<sub>25</sub>Cr<sub>21</sub>Mo<sub>8</sub>W<sub>Nb</sub>3C<sub>2</sub> prepared by mechanical alloying and hot pressing sintering. *Mater. Sci. Eng. A* **2018**, *728*, 144–150. [[CrossRef](#)]
77. Moravcik, I.; Cizek, J.; Zapletal, J.; Kovacova, Z.; Vesely, J.; Minarik, P.; Kitzmantel, M.; Neubauer, E.; Dlouhy, I. Microstructure and mechanical properties of Ni<sub>1.5</sub>Co<sub>1.5</sub>CrFeTi<sub>0.5</sub> high entropy alloy fabricated by mechanical alloying and spark plasma sintering. *Mater. Des.* **2017**, *119*, 141–150. [[CrossRef](#)]

78. Niinomi, M. Mechanical properties of biomedical titanium alloys. *Mater. Sci. Eng. A* **1998**, *243*, 231–236. [[CrossRef](#)]
79. Lu, J.W.; Zhao, Y.Q.; Ge, P.; Niu, H.Z.; Zhang, Y.S.; Zhang, W.; Zhang, P.X. Microstructure and mechanical properties of new high strength beta-titanium alloy Ti-1300. *Mater. Sci. Eng. A* **2015**, *621*, 182–189. [[CrossRef](#)]
80. Chen, J.; Zhang, C.; Cui, X.; Zhang, S.; Chen, J.; Zhang, J. Microstructure and corrosion behaviors of FeCrNiBSiMox stainless steel fabricated by laser melting deposition. In *Materials and Corrosion*; John Wiley & Sons, Inc.: Hoboken, NJ, USA, 2019; pp. 1–13.
81. Zadi-Maad, A.; Rohib, R.; Irawan, A. Additive manufacturing for steels: A review. *IOP Conf. Ser. Mater. Sci. Eng.* **2018**, *285*, 12028. [[CrossRef](#)]
82. Lin, K.; Gu, D.; Xi, L.; Yuan, L.; Niu, S.; Lv, P.; Ge, Q. Selective laser melting processing of 316L stainless steel: effect of microstructural differences along building direction on corrosion behavior. *Int. J. Adv. Manuf. Technol.* **2019**, *104*, 2669–2679. [[CrossRef](#)]
83. Hlinka, J.; Kraus, M.; Hajnys, J.; Pagac, M.; Petrů, J.; Brytan, Z.; Tański, T. Complex Corrosion Properties of AISI 316L Steel Prepared by 3D Printing Technology for Possible Implant Applications. *Materials* **2020**, *13*, 1527. [[CrossRef](#)]
84. Sarkar, S.; Sarswat, P.K.; Free, M.L. Elevated temperature corrosion resistance of additive manufactured single phase AlCoFeNiTiV0.9Sm0.1 and AlCoFeNiV0.9Sm0.1 HEAs in a simulated syngas atmosphere. *Addit. Manuf.* **2019**, *30*, 100902. [[CrossRef](#)]
85. Popov, V.V.; Katz-Demyanetz, A.; Koptuyg, A.; Bamberger, M. Selective electron beam melting of Al0.5CrMoNbTa0.5 high entropy alloys using elemental powder blend. *Heliyon* **2019**, *5*, e01188. [[CrossRef](#)] [[PubMed](#)]
86. Melia, M.A.; Whetten, S.R.; Puckett, R.; Jones, M.; Heiden, M.J.; Argibay, N.; Kustas, A.B. High-throughput additive manufacturing and characterization of refractory high entropy alloys. *Appl. Mater. Today* **2020**, *19*, 100560. [[CrossRef](#)]
87. Moorehead, M.; Bertsch, K.; Niezgodá, M.; Parkin, C.; Elbakhshwan, M.; Sridharan, K.; Zhang, C.; Thoma, D.; Couet, A. High-throughput synthesis of Mo-Nb-Ta-W high-entropy alloys via additive manufacturing. *Mater. Des.* **2020**, *187*, 108358. [[CrossRef](#)]
88. Kuncce, I.; Polanski, M.; Bystrzycki, J. Structure and hydrogen storage properties of a high entropy ZrTiVCrFeNi alloy synthesized using Laser Engineered Net Shaping (LENS). *Int. J. Hydrogen Energy* **2013**, *38*, 12180–12189. [[CrossRef](#)]



© 2020 by the authors. Licensee MDPI, Basel, Switzerland. This article is an open access article distributed under the terms and conditions of the Creative Commons Attribution (CC BY) license (<http://creativecommons.org/licenses/by/4.0/>).